View metadata, citation and similar papers at core.ac.uk

brought to you by CORE

provided by Elsevier - Publisher Connector

Biochimica et Biophysica Acta 1813 (2011) 1144–1152

Contents lists available at ScienceDirect

Biochimica et Biophysica Acta

journal homepage: www.elsevier.com/locate/bbamcr

Changes in mitochondrial redox state, membrane potential and calcium precede mitochondrial dysfunction in doxorubicin-induced cell death

Andrey V. Kuznetsov [a,*], Raimund Margreiter [b], Albert Amberger [c], Valdur Saks [d], Michael Grimm [a]

[a] Cardiac Surgery Research Laboratory, Department of Heart Surgery, Innsbruck Medical University, Innrain 66, Innsbruck A-6020, Austria
[b] Department of Visceral, Transplant and Thoracic Surgery, Innsbruck Medical University (IMU), Innsbruck A-6020, Austria
[c] Section of Human Genetics, Innsbruck Medical University (IMU), Innsbruck A-6020, Austria
[d] Laboratory of Fundamental and Applied Bioenergetics, INSERM U884, University Joseph Fourier (UJF), Grenoble, France

ARTICLE INFO

Article history:
Received 20 December 2010
Received in revised form 9 February 2011
Accepted 3 March 2011
Available online 13 March 2011

Keywords:
Confocal imaging
Doxorubicin
Mitochondria
Mitochondrial function
Redox state
Reactive oxygen species, ROS

ABSTRACT

Mitochondria play central roles in cell life as a source of energy and in cell death by inducing apoptosis. Many important functions of mitochondria change in cancer, and these organelles can be a target of chemotherapy. The widely used anticancer drug doxorubicin (DOX) causes cell death, inhibition of cell cycle/proliferation and mitochondrial impairment. However, the mechanism of such impairment is not completely understood. In our study we used confocal and two-photon fluorescence imaging together with enzymatic and respirometric analysis to study short- and long-term effects of doxorubicin on mitochondria in various human carcinoma cells. We show that short-term (<30 min) effects include i) rapid changes in mitochondrial redox potentials towards a more oxidized state (flavoproteins and NADH), ii) mitochondrial depolarization, iii) elevated matrix calcium levels, and iv) mitochondrial ROS production, demonstrating a complex pattern of mitochondrial alterations. Significant inhibition of mitochondrial endogenous and uncoupled respiration, ATP depletion and changes in the activities of marker enzymes were observed after 48 h of DOX treatment (long-term effects) associated with cell cycle arrest and death.
© 2011 Elsevier B.V. All rights reserved.

1. Introduction

Mitochondria play a central role in energy supply for normal cell function and also perform many important cellular tasks, such as induction of apoptosis and programmed cell death, cellular calcium and redox homeostasis [1,2]. On the other hand, important cellular functions of mitochondria are significantly changed in tumor cells and during chemotherapy [3–5]. Many recent reports show energy metabolism impairment and mitochondrial alterations to play a critical role in tumor progression and resistance to anticancer therapy [4,6]. However, conflicting data were frequently observed and also demonstrate a clear drug and cell type specificity. Doxorubicin (DOX) is known as a powerful anthracycline antibiotic widely used to treat many human cancers [7,8], but significant cardiotoxicity limits its clinical application [9–14]. Mitochondria are considered to be one of the primary targets of DOX through mitochondria-mediated apoptosis, remarkable modification of mitochondrial membranes (e.g. via binding with cardiolipin), which is also associated with changes in various mitochondrial functional parameters and activities of respiratory chain complexes like complex IV, complex III, phosphate carrier, etc. [15–21]. In addition, an involvement of DOX-induced oxidative stress has been evidenced by ROS overproduction, alterations in cellular redox state [9,12,17,22,23], diminished ROS-scavenging activities (e.g. catalase and glutathione peroxidase) and also by protective effects of various antioxidants such as Mito-Q [24], melatonin [25] and others. Moreover, doxorubicin significantly damages energy-transferring and -signalling systems like creatine kinase and AMP-activated protein kinase [26,27]. Also, it is known that DOX treatment may cause adaptive responses through the mitochondria and various cellular antioxidant defence systems, potentially contributing to the occurrence of multidrug resistance [28–30]. However, the detailed mechanisms by which doxorubicin interfere with mitochondrial function and cellular bioenergetics and, in particular, the exact sequence and metabolic impact of distinct events during DOX treatment remain largely unknown.

This study, using confocal fluorescence microscopy of mitochondrial flavoproteins and NADH, high-resolution respirometry of intact cells and analysis of key mitochondrial and non-mitochondrial enzymes, separately investigated various short- and long-terms effects of doxorubicin on mitochondrial functional and enzymatic parameters in various human carcinoma cells, including colorectal adenocarcinoma HT-29, DLD-1 and HRT-18 cells, breast tumor MCF-7 and Hs578-T cells. Taken together, our data demonstrate that DOX treatment results in several patterns of mitochondrial change: 1) rapid, early effects were a remarkable shift towards a more oxidized state of mitochondria, 2) decrease in the inner mitochondrial membrane potential and 3) elevated mitochondrial calcium level. These changes preceded

Abbreviations: DCF-DA, 2′,7′-dichlorodihydrofluorescein diacetate; DOX, doxorubicin; FCCP, carbonyl cyanide *p*-trifluoromethoxyphenyl-hydrazone; ROS, reactive oxygen species; TMRE, tetramethylrhodamine ethyl ester; UCR, uncoupling control ratio

* Corresponding author. Tel.: +43 512 504 27815; fax: +43 512 504 27805.
E-mail address: andrey.kuznetsov@uki.at (A.V. Kuznetsov).

0167-4889/$ – see front matter © 2011 Elsevier B.V. All rights reserved.
doi:10.1016/j.bbamcr.2011.03.002

alterations in mitochondrial respiratory function, cellular ATP levels and enzymatic activities (long-term effects). In addition, we show that mitochondrially located ROS can also be detected rapidly after DOX addition, most probably due to respiratory chain-produced superoxide radicals. On the other hand, ROS overproduction and oxidative stress can also be related to a different mechanism.

2. Materials and methods

2.1. Cell culture

Human colon cancer HRT-18 and HT-29 cell lines and breast cancer MCF-7 and Hs578-T cell lines obtained from American Type Culture Collection were used in this study (in some experiments colon carcinoma DLD-1 cells were also used). Cells were routinely cultured in RPMI-1640 growth medium supplemented with antibiotics, glutamine and 10% FCS. New cultures were re-established from frozen stocks every 3 months. Once a month routine tests were conducted to confirm that cells were free of mycoplasm (mycoplasm detection kit, Stratagene, Amsterdam, The Netherlands). For experiments, cells were detached with trypsin, washed once in medium, and seeded in falcon flasks (12 ml). For respiration and enzymatic analysis, cells were cultured for 48 h in growth medium in the absence or presence of various concentrations of doxorubicin. Cells were then detached with trypsin, washed, resuspended in the growth medium ($1–2 \times 10^6$ cells/ml) and used for further analysis. In confocal imaging experiments, cells were incubated with doxorubicin using LAB-TEK® chambered microscopic cover-glasses ("Nalge-Nunc International", Naperville, USA). Parental MCF-7 cell lines were grown in MEM medium, supplemented with 10% FCS, 50 μg/ml penicillin–streptomycin, 2 mM L-glutamine, and 1 mM sodium pyruvate (PAA, Linz, Austria) and maintained at 37 °C in a humidified atmosphere containing 5% CO_2.

2.2. Cell size, count and viability

Casy®-1 Cell Counter and Analyser System model TT (Schärfe System, Reutlingen, Germany) was used to measure cell size profiles (cell count versus cell size), maximal and mean values of cell diameters, volumes and cell viability. For this purpose, 100 μl of cell suspension was added to 10 ml of measuring buffer. In addition, a routine trypan blue test was always used to count viable and non-viable cells.

2.3. FACS analysis

Flow cytometric analysis of cells stained with propidium iodide (50 μg/ml) was performed using the Becton Dickinson Cytometry System and CellQuest software. For each analysis, 20,000–30,000 gated events were collected. Cell cycle analysis was performed using Modfit LT (Verity Software House).

2.4. Enzymatic analysis

Three essential enzymes were chosen for the analysis. The activity of two marker mitochondrial enzymes was assayed: mitochondrial matrix enzyme citrate synthase (CS) and respiratory chain enzyme NADH:ubiquinone oxidoreductase (Complex I) located in the inner mitochondrial membrane. In addition, the activity of cytosolic enzyme lactate dehydrogenase (LDH) was also measured. Activities of all enzymes were determined in cells frozen in liquid nitrogen and stored at −80° C using spectrophotometry at 30° C in medium supplemented with 0.1% Triton X-100 [31,32].

2.5. Measurement of cellular ATP content

Cellular ATP content was measured using the luceroferin-luceroferase system (bioluminescent cell assay kit, "Sigma") and multiplate luminometer. ATP was extracted from cells after protein precipitation using 0.5 M perchloric acid and subsequent neutralization with 1 M K_2CO_3 and 100 mM HEPES-K (pH 7.4), following centrifugation at 10,000*g* for 5 min to remove precipitates. The ATP calibration curve was used for final analysis.

2.6. Cellular respiration

Oxygen consumption of the cells was measured with a titration-injection respirometer (OROBOROS® *Oxygraph*, Innsbruck, Austria) in RPMI growth medium [33], before and after addition of the mitochondrial uncoupler FCCP (2–4 μM) at 30 °C, assuming an O_2 solubility of 10.5 μmol l^{-1} kPa^{-1} (1.4 μmol l^{-1} $mmHg^{-1}$). DatLab software (Oroboros, Innsbruck, Austria) was used for data acquisition and analysis. Respiration rates were expressed in pmol of O_2 per second, per 10^6 cells. Both endogenous and uncoupled respiration rates were linearly dependent on the cell density in range $0.1–6 \times 10^6$ cells/ml. Also, mitochondria-specific inhibitors blocked respiration confirming that oxygen consumption was due to the respiratory chain (data not shown).

2.7. Measurement of ROS production

ROS production was measured by loading cells with 20 μM DCF-DA (2,7-dichlorodihydrofluorescein diacetate) or with 5 μM MitoSOX™ Red for 30 min at room temperature in the dark. After washing with PBS, cells were further processed for analysis using spectrofluorimetry or confocal microscopy [34]. ROS production was measured using a Shimadzu RF-5301PC spectroflourophotometer at room temperature and results were expressed as arbitrary units (a.u.) per min, per 10^6 cells. Fluorescence intensity was linearly proportional to cell concentration up to 5×10^6 cells per ml (data not shown).

2.8. Confocal imaging of mitochondrial redox state (autofluorescence of mitochondrial flavoproteins and NADH)

Mitochondrial flavoprotein and NADH autofluorescence were imaged simultaneously [35–38] using a confocal microscope (LSM510 NLO, Zeiss) with a 40× (NA 1.2) water immersion lens. The use of such a water immersion objective prevented geometric aberrations. The autofluorescence of flavoproteins was excited with the 488-nm line of an argon laser, and the laser output power was set to an average of 8 mW (about 60%). Fluorescence was collected through a 510-nm dichroic beam splitter and a 505- to 550-nm band-pass filter. The pinhole aperture was set to one Airy disk unit. NADH autofluorescence was imaged by means of two-photon excitation using a femtosecond pulsed infra-red laser (Tsunami + MilleniaVIII, SpectraPhysics). Pulse frequency was set at 100 MHz with a pulse width of 100 fs. The infra-red line was tuned to 720 nm. Laser output power was set to 400 mW (70%). The fluorescence signals were collected through a multi-line beam splitter with maximum reflections at 488 ± 10 nm (for rejection of the 488-nm line) and above 700 nm (for rejection of infra-red excitation). A second 490-nm beam splitter was used to discriminate the NADH signal from the flavoprotein signal. Then the flavoprotein signal was passed through a 500- to 550-nm band-pass filter with an additional infra-red rejection filter before being collected through a pinhole (one Airy disk unit). The NADH signal was redirected to a 390- to 465-nm band-pass filter with an additional infra-red rejection filter.

2.9. Imaging analysis of mitochondrial membrane potential and mitochondrial calcium

In order to analyze mitochondrial distribution and mitochondrial inner membrane potential, cells were incubated for 30 min at room temperature with 50 nM tetramethylrhodamine ethyl ester (TMRE). TMRE fluorescence was excited with a 543-nm helium-neon laser; the

laser output power was set to 1 mW. For colocalization studies the fluorescence signals were collected through a multi-line beam splitter with maximum reflections at 488 ± 10 nm (for rejection of the 488-nm line) and at 543 nm (for rejection of the 543-nm line). A second 545-nm beam splitter was used to discriminate the TMRE signal from the flavoprotein signal. Then the flavoprotein signal was passed through a 505-nm long-pass filter before being collected through a pinhole (one Airy disk unit). The TMRE signal was redirected to a 560-nm long-pass filter before being collected through a pinhole (one Airy disk unit). To analyze the level of mitochondrial matrix calcium, cells were preloaded with fluorescent Ca^{2+}-specific probe Rhod-2. For this, cells were incubated for 30 min at room temperature with 5 μM Rhod-2. Rhod-2 has a net positive charge allowing its specific accumulation in mitochondria. Confocal imaging of Rhod-2 fluorescence was performed as described for TMRE. Rhod-2 as TMRE fluorescence was also imaged simultaneously with flavoprotein and NADH fluorescence. Time series were acquired during 0–30 min with 30 s intervals. The notion that TMRE and Rhod-2 are specific mitochondrial indicators was evidenced by their full colocalization with mitochondrial flavoproteins as integral components of the mitochondrial inner membrane and mitochondria-specific probe MitoTracker Green (data not shown).

2.10. Imaging of ROS production

ROS production was visualized in cells loaded with 20 μM of 2′,7′-dichlorodihydrofluorescein diacetate, (DCF-DA, Sigma) for 20 min at room temperature. ROS-induced green fluorescence of DCF was imaged using 488-nm laser excitation. The laser power was set to 1–3%. Importantly, this power setting allowed complete discrimination of DCF fluorescence and the autofluorescence originating from the oxidized form of mitochondrial flavoproteins. The 515- to 530-nm emission range was used to monitor an increase in dichlorofluorescein, the oxidized product of DCF-DA.

2.11. Quantitative assessments of the fluorescence signal

In all imaging studies the intensity of fluorescence (grey value) was analyzed in the areas of interest (mitochondria-rich areas) using "Scion Image" software for Windows (Release Beta 4.0.2. NIH, USA). Background fluorescence (no cells area) was subtracted from the corresponding signal. In each measurement ($n = 3$–6), fluorescent signals from 4 to 6 mitochondria-rich areas (in regions of interest, Roi) of 10–20 cells were averaged.

2.12. Reagents

Rhod-2 was obtained from "Molecular Probes Inc." (Leiden, The Netherlands); other reagents (TMRE, DCF-DA, etc.) were purchased from "Sigma" (Vienna, Austria).

2.12.1. Data analysis

All data are presented as means ± SD. Statistical analyses were performed using Student's *t*-test and $P<0.05$ was taken as the level of significance.

3. Results

3.1. Effects on cell size, cell cycle and viability

Mitochondrial confocal imaging, enzymatic and high-resolution respirometry approaches were used to study multiple effects of doxorubicin (short- and long-term) on various important parameters of mitochondria and to correlate these with cell viability. Short treatment of cells with doxorubicin (less than 1 h of incubation, DOX concentration range: 1–10 μg/ml) had no effect on cell viability (data not shown). Alternatively, prolonged incubation with the drug resulted in time- and concentration-dependent cell death and detachment (up to 90% cells after >48 h of incubation following incubation with 10μg/ml DOX) in all cell types used in the study (Fig. 1A). This cell detachment was always in parallel with a decrease in cell viability analyzed by trypan blue staining (Fig. 1B) and with increased percentage of dead cells using flow cytometry (FACS) and propidium iodide (PI) staining. It was recently reported that DOX inhibits cell proliferation via cell cycle arrest in the G(2)/M phase in murine lymphocytes [39]. Similar to this study, when using FACS analysis we showed that doxorubicin treatment induced a concentration-dependent accumulation of the human carcinoma cells in the G(2)/M phase, demonstrating inhibition of cell proliferation by cycle arrest in this phase (Fig. 2). Using the Casy® Cell Counter and Analyser System, cell size profiles (cell count versus cell size) were analyzed and showed a significant shift in cell size distribution after incubation with DOX (cell diameter 15 ± 0.7μm and 17 ± 0.5μm, for control and DOX-treated but still attached MCF-7 cells, respectively, $P<0.01$). The measurements were performed after 48 h of incubation with the drug (10 μg/ml), showing similar changes for other cells used in the study (also in colon carcinoma cells). Modifications in cell morphology and size induced by DOX have been shown also in cultured leukemia cells [40].

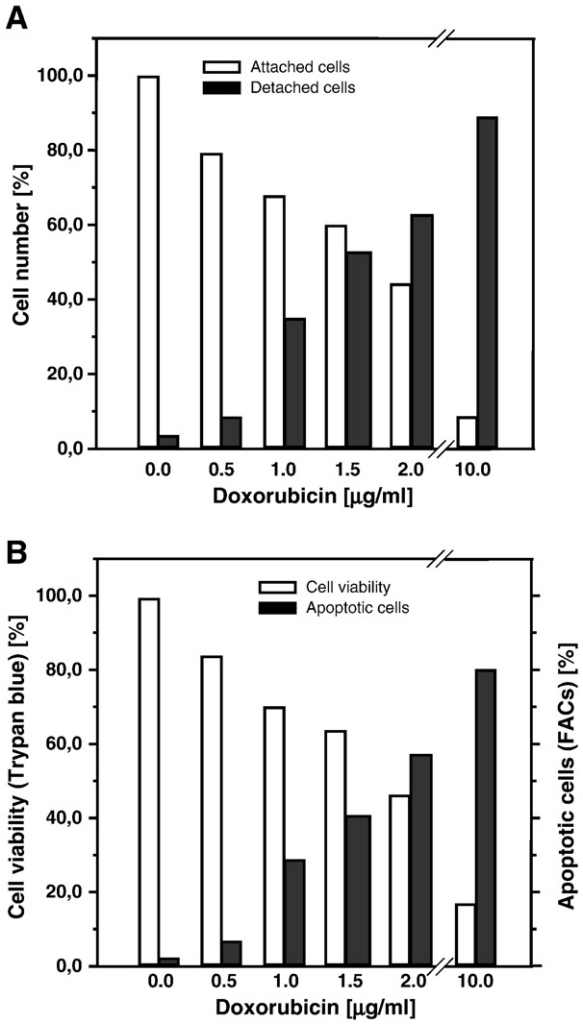

Fig. 1. Effect of various doxorubicin concentrations on cell detachment (A) and viability (B). MCF-7 (A) or DLD-1 (B) cells were incubated 48 h with different DOX concentrations in RPMI-1640 medium. (B) Cell viability was estimated by trypan blue assay, degree of cell death was determined by flow cytometry using propidium iodide (PI) staining.

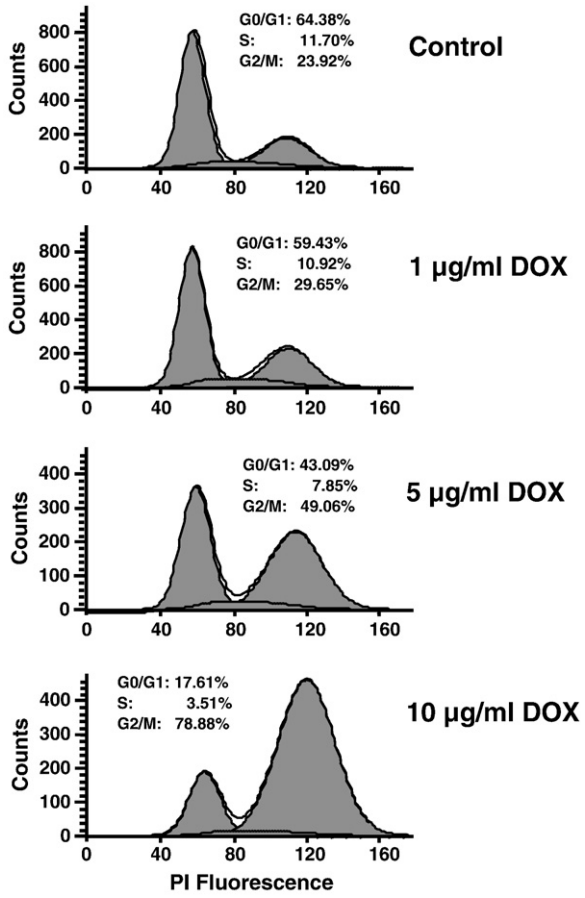

Fig. 2. FACS analysis of the effect of various doxorubicin concentrations on cell cycle in human breast carcinoma Hs578-T cells. Incubation with doxorubicin (48 h) resulted in a significant dose-dependent increase in cells arrested in the G2/M phase of the cell cycle. (A) Control. (B) 1.0 μg/ml doxorubicin. (C) 5.0 μg/ml doxorubicin. (D) 10 μg/ml doxorubicin.

3.2. Confocal imaging of rapid changes in the mitochondrial redox state, in the inner membrane potential and mitochondrial matrix calcium

The mitochondrial confocal imaging approach was used for rapid analysis of fast changes in several important mitochondrial parameters in living, confluent cells after addition of DOX (Fig. 3A–D). Simultaneous confocal imaging of mitochondrial flavoproteins and NADH autofluorescence (using two-photon excitation) as redox state indicators, Rhod-2 fluorescence as indicator of mitochondrial matrix calcium, and TMRE fluorescence as sensor of the mitochondrial inner membrane potential in human carcinoma cells demonstrated remarkable and rapid (<30 min) changes in these parameters after addition of 10 μg/ml DOX (Fig. 3C). Quantification of the results of these experiments, including statistics, is summarized in Table 1. It can be seen that in all cell types used in the study, doxorubicin treatment resulted in a significant (almost 2-fold) increase in autofluorescence intensity of mitochondrial flavoproteins (green, fluorescent in oxidized state), together with a clear decline in the NADH autofluorescence signal (blue, only fluorescent in its reduced state), both indicating oxidation of these two important markers of the mitochondrial redox state and thus showing rapid transition of mitochondria to their significantly more oxidized state (Fig. 3C, Table 1). Moreover, simultaneous monitoring of TMRE fluorescence demonstrated that doxorubicin treatment also resulted in a quick drop in membrane potential (Fig. 3D), visible as a strong decline in fluorescence intensity, as a result of less mitochondrial membrane potential and decreased sequestration of this potentiometric-sensitive dye. In parallel sets of experiments, an increase in the mitochondrial matrix calcium was observed from the remarkable increase in fluorescence intensity of the mitochondrial calcium-sensitive probe Rhod-2 (Fig. 3C) parallel to the changes described above. Importantly, all cell types (MCF-7, HTR-18, HT-29 and Hs578-T) exhibited a similar extent and patterns of changes (Table 1).

3.3. Mitochondrial respiratory function and coupling in DOX-treated cells

Effects of DOX treatment on mitochondria were also estimated by measuring mitochondrial respiratory function as a sensitive indicator of cell injury and adaptation. Importantly, no changes in mitochondrial respiration were found after brief incubation (<1 h) with DOX following addition of the drug to the oxygraph chamber during respiration measurement (or titration with DOX in the range of 1–10 μg/ml, data not shown). In contrast, long-term cell exposure to DOX (48 h) significantly decreased rates of mitochondrial respiration (Fig. 4A). Moreover, FCCP-stimulated uncoupled respiration was also significantly decreased, reflecting diminished respiratory capacity of mitochondria in intact cells. Notably, most pronounced decline was observed in breast carcinoma MCF-7 cells (Fig. 4A). From these experiments, in addition to information on absolute respiratory fluxes (endogenous and uncoupled), the uncoupling control ratio (UCR), a parameter showing the degree of respiratory stimulation by FCCP, was also derived. This ratio was also significantly reduced after DOX treatment (Fig. 4B). Again, more pronounced decline in UCR was observed in MCF-7 cells (from 3.60 ± 0.09 to 1.90 ± 0.11).

3.4. Effects of DOX on cellular ATP level

Consistent with the results of mitochondrial respiration analysis showing functionally disturbed mitochondria after long-term (48 h) DOX treatment, incubation with DOX also resulted in a significant decline in cellular ATP content measured after the same treatment time (Fig. 4C). Certainly, this decline can be a consequence of both the lower rates of mitochondrial respiration and the lower efficacy (coupling) of oxidative phosphorylation observed in the study.

3.5. Enzymatic analysis of DOX-treated cells

In addition to imaging analysis and high-resolution respirometry, changes in the activities of key marker mitochondrial and non-mitochondrial enzymes were tested in carcinoma cells after long-term incubation (48 h) with DOX. This analysis included an assessment of the activities of mitochondrial matrix enzyme citrate synthase (CS), mitochondrial respiratory complex I and cytosolic enzyme LDH (Table 2). It can be seen that DOX treatment remarkably diminished the activity of respiratory complex I in MCF-7 cells, while the activities of other tested enzymes in DOX-treated but still attached carcinoma cells were not significantly changed (Table 2).

3.6. Detection of DOX-induced ROS production

Significantly more oxidized states of mitochondrial flavoproteins and NADH observed after short-term treatment with DOX (20–30 min, see above) are well consistent with mitochondrial ROS generation detected by the fluorescent indicator DCF-DA using both confocal microscopy and spectrofluorometry (Fig. 5; for isolated cardiomyocytes see also ref. [41]). Confocal imaging analysis of DCF-DA fluorescence in cells double-loaded with DCF-DA and mitochondrial membrane potential-sensitive probe TMRE demonstrated that DOX-induced ROS production in human carcinoma cells is mostly colocalized with mitochondria (Fig. 5A), indicating a mitochondrial origin of the DOX-induced ROS. Moreover, using spectrofluorometry analysis and the same ROS indicator we show that the mitochondrial uncoupler FCCP

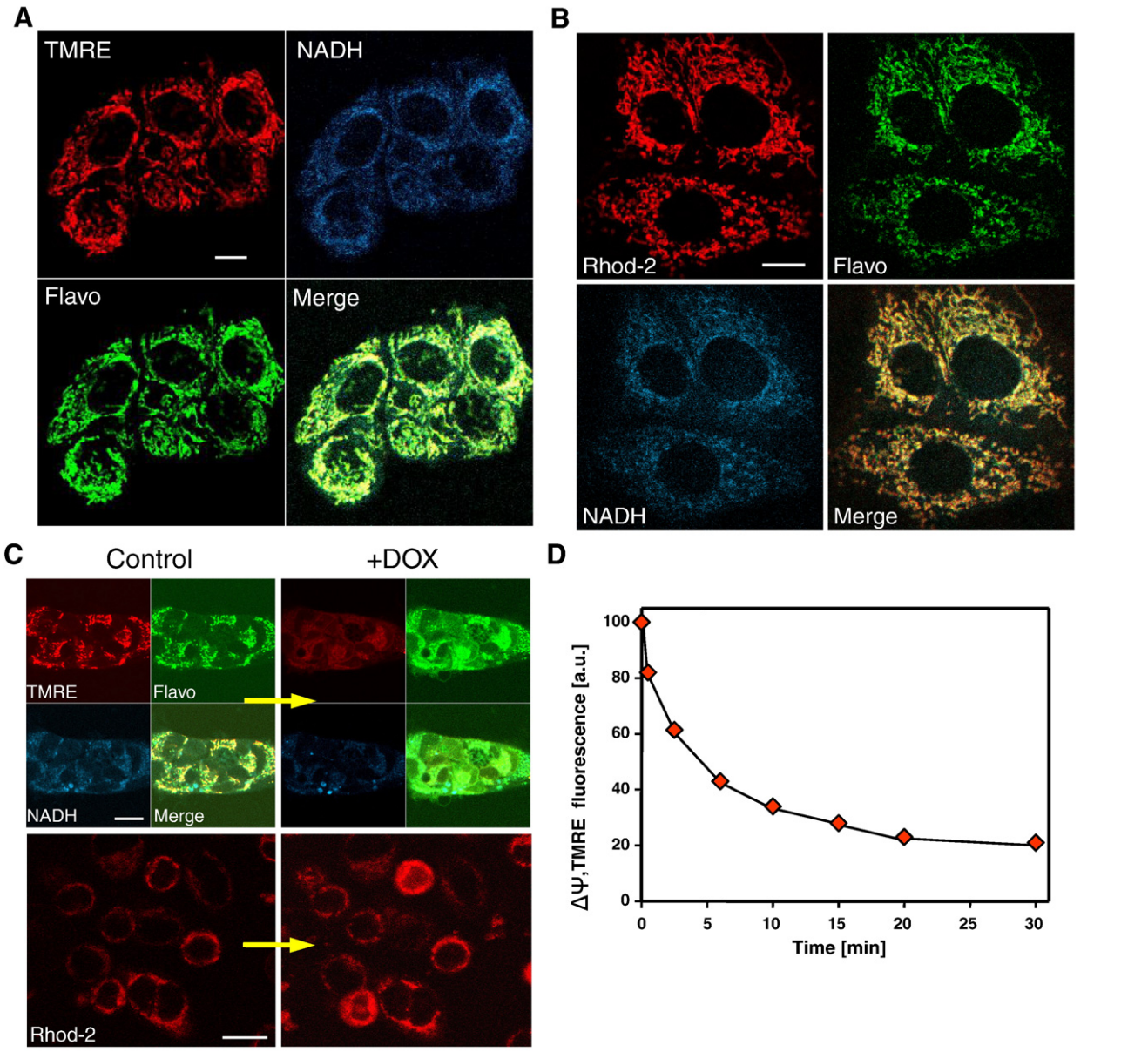

Fig. 3. Representative confocal imaging of mitochondrial functional changes in MCF-7 cells after DOX treatment. (A) Simultaneous imaging of autofluorescence of mitochondrial flavoproteins (flavo, green) and NADH (blue) as mitochondrial redox state indicators and fluorescence of TMRE as inner membrane potential-sensitive probe. (B) Simultaneous imaging of mitochondrial flavoproteins (flavo) and NADH and mitochondrial matrix calcium (cells were stained with Rhod-2). Scale bar = 10 μm. (C) Upper panel, representative changes in fluorescence of flavoproteins (flavo), NADH and TMRE after 20 min of incubation with DOX. Lower panel, representative changes in fluorescence of mitochondrial calcium indicator Rhod-2 after 20 min of incubation with DOX. Bar, 20 μm. (D) Representative time-course (kinetics) of DOX effect on mitochondrial inner membrane potential (ΔΨ) analyzed by monitoring of TMRE fluorescence (a.u., arbitrary units).

significantly decreased ROS production by dissipating mitochondrial membrane potential, whereas the inhibitor of mitochondrial complex III, antimycin A, stimulated ROS production (Fig. 5B), thus also pointing to the mitochondrial origin of ROS. Similar results were obtained using another ROS-sensitive probe MitoSOX™ Red (data not shown). However, some generation of non-mitochondrial ROS can not be completely excluded, for example by membrane-bound NADPH oxidase (NOX) [42], or due to direct involvement of ROS-producing DOX chemistry [17,22].

4. Discussion

Doxorubicin (DOX) is a widely used chemotherapeutic drug for the treatment of acute leukemia, lymphomas and different types of solid tumor, but it can produce complications leading also to multidrug resistance. Although the mitochondrial dysfunction and the severe inhibition/inactivation of certain mitochondrial systems have been implicated as important pathways of the DOX action associated with its remarkable cardiotoxicity (cardiomyopathy), the exact molecular mechanisms are still unclear. Using colon HT-29 and HRT-18 and mamma MCF-7 and Hs578-T cancer cell lines we confirmed previous findings observed in murine lymphocytes [39], namely that DOX inhibits cell proliferation through cell cycle arrest at the G(2)/M phase (Fig. 2) in a time- and dose-dependent manner, also causing massive cell death (Fig. 1B).

Simultaneous imaging of autofluorescence of mitochondrial flavoproteins and NADH (two-photon excitation) as sensitive indicators of mitochondrial redox potentials [43,44] was performed at the single cell and single organelle level in response to short-term (20–30 min) DOX treatment. Importantly, the redox state of flavoproteins located in the inner mitochondrial membrane is in balanced equilibrium with the redox state of mitochondrial NAD(P)H [38]. Accordingly, a rapid strong

Table 1
Quantitative analysis of alterations in fluorescence intensity of mitochondrial flavoproteins, NADH, TMRE and Rhod-2 in various human carcinoma cells after short-term incubation with doxorubicin.

Cell type	Flavoproteins	NADH	TMRE	Rhod-2
MCF-7	165.5 ± 28.0**	83.4 ± 3.9**	26.8 ± 1.5***	161.2 ± 38.6**
Hs578-T	148.0 ± 12.5**	80.5 ± 2.9**	67.6 ± 1.7***	n.d.
HRT-18	135.5 ± 9.3**	90.5 ± 18.9	60.8 ± 6.3***	135.2 ± 9.8*
HT-29	150.5 ± 14.9**	88.2 ± 7.7	49.8 ± 2.3***	n.d.

Fluorescence intensity was measured before and after cells incubation with DOX (10 μg/ml, 20 min) in chambered microscopic cover-glasses, as grey value in the mitochondria-rich areas (regions of interest, Roi) within cells, using inverted confocal fluorescent images and the "Scion Image for Windows" program. Values are given as percentage of the corresponding controls (before DOX addition) and after background fluorescence correction. Data for 4–6 cell areas in 10–20 different cells are averaged. ± shows SD; n = 4–6; significantly different from corresponding controls, *P<0.05, **P<0.01, ***P<0.001. n.d., not determined.

Table 2
Changes in the enzyme activities of mitochondrial matrix enzyme citrate synthase (CS), mitochondrial respiratory chain complex I and cytoplasmic enzyme lactate dehydrogenase (LDH) in DOX-treated human carcinoma cells (long-term effects).

Cell type	Complex I	CS	LDH
MCF-7 control	29 ± 9	67 ± 20	130 ± 30
+ DOX	13 ± 3**	61 ± 17	166 ± 40
Hs578-T control	20 ± 5	66 ± 16	92 ± 8
+ DOX	18 ± 7	60 ± 17	60 ± 17
HT-29 control	n.d.	69 ± 15	54 ± 19
+ DOX		71 ± 20	55 ± 19
DLD-1 control	n.d.	55 ± 11	35 ± 11
+ DOX		63 ± 20	37 ± 9

Enzyme activities are given in mU per 10^6 cells. Cells were incubated with doxorubicin (10μg/ml) for 48 h at 37 °C in the culture medium. Enzyme activities were measured at 37 °C as described in the "Materials and methods" section. ± shows SD; n = 3–6; **significantly different from corresponding control, P < 0.01. n.d., not determined.

increase in flavoprotein fluorescence (changes in its redox potentials) after DOX addition was seen parallel with a remarkable decrease in mitochondrial NADH fluorescence (Fig. 3A, Table 1), both reflecting a general shift of mitochondria towards their more oxidative state. Notably, due to cross-talk between mitochondrial and cytoplasmic NAD(P)H this shift may lead to significant alterations (perturbations), also in the overall cellular redox state. Moreover, cellular dehydrogenases and various metabolic pathways continuously produce NAD(P)H, which may operate directly as an intracellular antioxidant as long as it is regenerated [45]. However, our confocal microscopy imaging study showed that both NAD(P)H and flavoprotein fluorescence exhibited a predominant localization in mitochondria (Fig. 3A and B). We demonstrated that the intensity of both fluorescence signals was sensitive to DOX treatment and also to changes in the mitochondrial metabolic state, like the presence or absence of mitochondrial substrates [35,37,38,46,47], inhibitors, different concentrations of oxygen, as well as to changes in different models of cell injury [48]. Both the cellular redox state and the overall cellular NAD(P)H pull depend on the complex interrelations of many cellular systems [45]. The regenerative function of many antioxidative and ROS-scavenging enzymes in the cell requires NADH or NADPH, both of which are produced by various dehydrogenases and by the mitochondrial Krebs cycle. Moreover, the transient oxidation of NAD(P)H and thus changes in the cell redox state can be closely associated with a decrease in total cellular antioxidant capacity as well as with an increase in mitochondrial or non-mitochondrial ROS production.

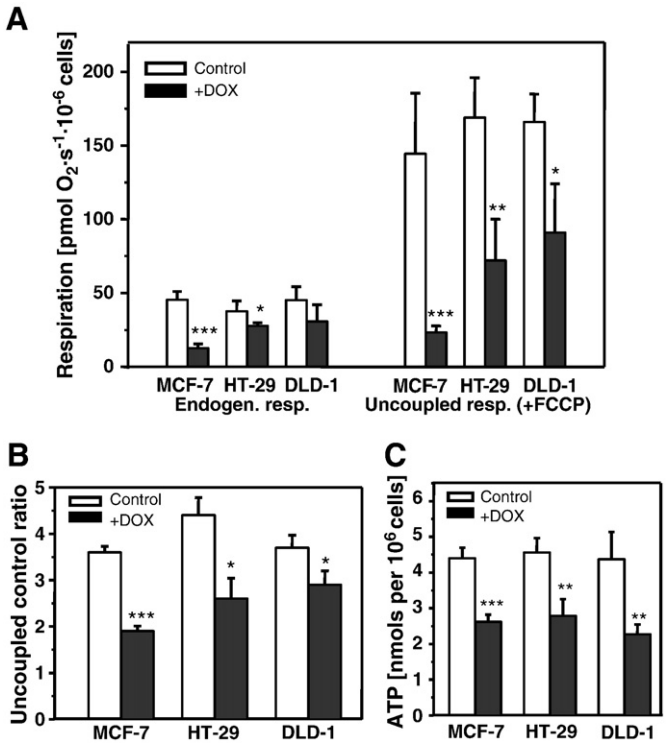

Fig. 4. Decrease in mitochondrial respiratory function and ATP content in various carcinoma cells after treatment with doxorubicin. (A) Respiration rates were measured at 37° C in control and DOX-treated cells after 48 h of incubation, before (endogenous respiration) and after addition of FCCP (uncoupled respiration). (B) The respiratory uncoupling ratio (UCR) was calculated as the ratio of uncoupled and endogenous respiration. (C) Cellular content of ATP in control and DOX-treated cells. Incubation conditions with DOX are described in "Materials and methods". Error bars show ± SD; n = 3–6; significantly different from corresponding controls: *P<0.05, **P<0.01, ***P<0.001.

Since the confocal imaging technique allows concomitant detection of fluorescence probes with different spectral characteristics, analysis of the redox state of mitochondria can be combined with imaging of mitochondrial membrane potential monitored by TMRE fluorescence (Fig. 3A), or mitochondrial matrix calcium analyzed by Rhod-2 fluorescence (Fig. 3B), both also colocalized with MitoTracker Green, specific for mitochondria (see "Materials and methods"). Using such a combined imaging approach we showed that the mitochondrial shift towards their more oxidized state took place parallel with significant mitochondrial depolarization (Fig. 3C and D), which occurs (as shown in separate experiments) simultaneously with an increase in mitochondrial calcium levels. Also, a rapid decrease in mitochondrial transmembrane potential (ΔΨm) was obtained using another potential-sensitive dye JC-1 [49]. In these experiments, authors show that, with the progression of exposure time, the early depolarization of the mitochondrial membrane was followed by a transient reversion to normal ΔΨm (see ref. [49]). Notably, calcium and ROS changes can also be transient in various carcinoma cells under laser-induced photo-oxidative stress (our unpublished data). It is well known that an accumulation of Ca^{2+} in mitochondria and a drop in mitochondrial membrane potential can be associated with ROS production and that both are prerequisite steps for the induction of mitochondrial permeability transition (MPT) and subsequent cell death by apoptosis or necrosis [50,51]. Also, the rapid rise in mitochondrial Ca^{2+} after doxorubicin addition observed in our study is well consistent with previous findings showing a greater than 2-fold increase in cytosolic Ca^{2+} in DOX-treated cultured cardiomyocytes [52,53]. These data suggest that doxorubicin-induced alterations in mitochondrial Ca^{2+} homoeostasis (see also [54]) are associated with a failed energy (ATP) production and thus a decrease in ATP level, further resulting in cell injury and cardiotoxicity.

To further define the effects of doxorubicin on mitochondria and cell energy metabolism, we measured cellular respiration (Fig. 4A and B) and ATP content (Fig. 4C). Cellular respiration rate reflects normal

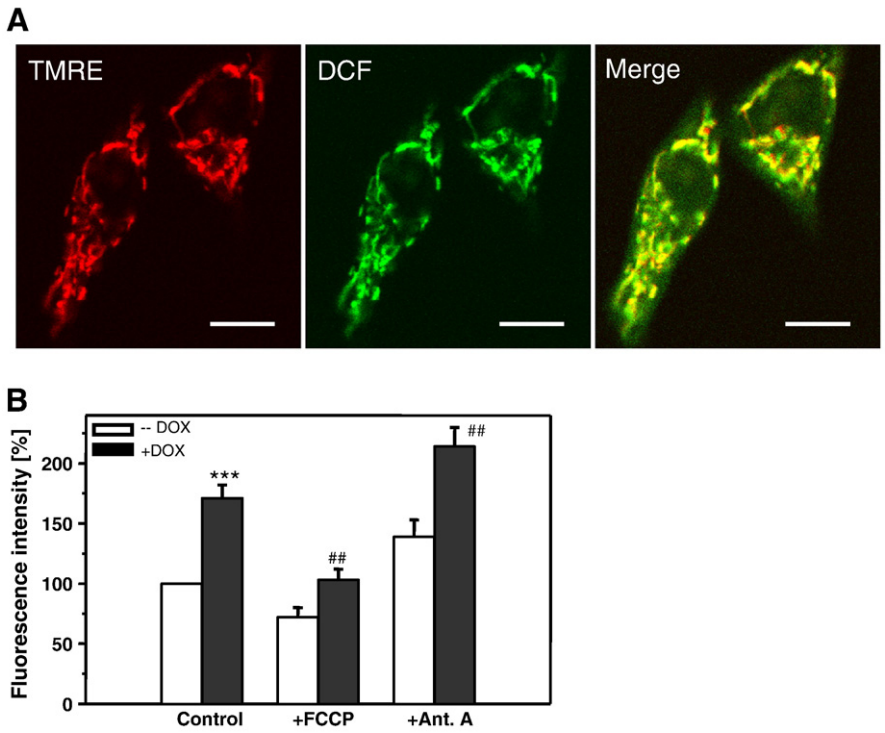

Fig. 5. DOX-induced mitochondrial ROS production. (A) Representative confocal imaging of DOX-induced mitochondrial ROS production in MCF-7 cells after 20 min of incubation with DOX. Cells were double-stained with 20 μM DCF-DA and 100 nM TMRE. Bar, 10 μm. (B) Effects of mitochondrial uncoupler FCCP and specific inhibitor of mitochondrial respiratory complex III antimycin A (Ant. A) on DOX-induced mitochondrial ROS production (closed bars). Error bars show ± SD; $n = 4$; significantly different from corresponding controls without DOX (open bars); $^{***}P<0.001$, $^{\#\#}P<0.01$.

mitochondrial respiratory function in intact cells and can be dependent on the factors of cellular metabolism like ADP concentration. Alternatively, FCCP-stimulated respiration reflects the maximal respiratory capacity of uncoupled mitochondria, which can also be dependent on availability and concentrations of various metabolites, substrates and Ca^{2+}. Importantly, a significant decline in respiration rates was observed only after long- but not short-term drug treatment. This indicates that initial changes in mitochondrial redox state, membrane potential and calcium, well visible with confocal imaging, had no effect on mitochondrial respiratory function. More probably, specific damage to or partial inhibition of mitochondrial respiratory chain complexes can be an expected explanation for the respiratory decline after long-term incubation. No significant changes in CS activity (frequently used marker of mitochondrial content, see Table 2) also point to a specific respiratory chain defect, rather than general loss of mitochondrial mass. Previous findings have shown mitochondrial dysfunction [55] and inactivation of mitochondrial systems such as complexes I, III, and IV (COX), and also phosphate carrier [18,20,21,56,57] and ATP-ADP translocase [58], due to binding of DOX to cardiolipin of the inner mitochondrial membrane [19,20,59]. This can remarkably contribute to the inhibition of mitochondrial activity in DOX-treated mitochondria [27,60]. Alternatively, in contrast to our and some other previous findings, in Jurkat and HL-60 cells, doxorubicin treatment increased cellular mitochondrial oxygen consumption after 24 h of exposure to the drug [61]. However, the same group showed contradicting results regarding effects of DOX on mitochondrial respiration, demonstrating that incubation of cells with high-dose doxorubicin (5–20 μM) caused a significant inhibition of mitochondrial respiration [62].

In addition to the information on absolute respiratory fluxes, an important ratio can be derived from our protocol. The uncoupling control ratio (UCR) is the ratio of the uncoupled rate of respiration to endogenous respiration, and this parameter also significantly declined in DOX-treated cells (Fig. 4B), consistently with previous findings obtained in DOX-treated cardiac mitochondria [54]. The UCR value reflects the respiratory reserve capacity, and it may decline due to increased ADP-stimulated endogenous respiration (e.g. because of higher energy demand), due to the uncoupling of mitochondria or to decreased respiratory capacity at constant endogenous respiration. Interestingly, cell treatment with DOX significantly changed the sensitivity of mitochondria to the mitochondrial uncoupler FCCP. Titration experiments using a stepwise increasing FCCP and that were routinely performed to define its optimal concentration (about 4 μM in control cells) demonstrated that a significantly greater concentration of FCCP was required in DOX-treated cells (about 20 μM) in order to obtain a stimulatory effect similar to that obtained in control cells. The titration curve was remarkably shifted to the right probably due to DOX-induced conformational changes in the mitochondrial inner membrane. Noticeably, the sensitivity to the uncoupler (FCCP) can be significantly dependent on the conformational state of the mitochondrial inner membrane (e.g. changes in its fluidity, regularity, etc.). On the other hand, it is well known that DOX may strongly interact with certain phospholipids of this membrane. In particular, DOX has a high affinity to cardiolipin [20,59,63], causing thus changes in membrane physicochemical properties. The significantly decreased ATP level found in DOX-treated cells (Fig. 4C) points to the major role of mitochondrial oxidative phosphorylation in maintaining energy status in human carcinoma cells despite the expected bioenergetic shift towards a more glycolytic pathway, which is a widely accepted characteristic of all cancers (Warburg effect), thus assuming a secondary role of mitochondria in ATP synthesis in tumors.

It has been demonstrated that DOX exposure leads to rapid reactive oxygen species (ROS) production by means of various mechanisms [9,22,52,55,64,65]. Many studies support the theory that mitochondria are a primary target of DOX-induced oxidative stress, both acute and long-term, and our findings are in good agreement with this concept. The role of ROS in DOX-induced cell death has been demonstrated using both in vivo and in vitro models [23]. Additional indirect evidence for ROS involvement is that DOX-induced cell death can be attenuated

by antioxidants and cell-permeable SOD. There is consensus that DOX cardiotoxicity is related to ROS induction with subsequent mitochondrial and cell injury [9,25,52]. Also, the mitochondrial origin of ROS can be partially confirmed by the cardioprotective effects of the specific mitochondria-targeting antioxidant Mito-Q during DOX-induced cardiomyopathy [24]. Our confocal imaging experiments, using DCF fluorescence as intracellular ROS indicator, demonstrate that ROS was rapidly produced upon DOX addition parallel with changes in mitochondrial redox state and membrane potential. Importantly, imaging analysis confirmed that ROS production in human carcinoma cells was mainly colocalized with mitochondria double-stained with DCF and specific mitochondrial probe TMRE (Fig. 5A). Also, clear effects of specific mitochondrial agents: uncoupler FCCP and inhibitor antimycin A on ROS generation further indicated their mitochondrial origin (Fig. 5B). However, from our data we can not distinguish whether DOX-induced ROS were direct causes of the more oxidized mitochondrial state and elevated Ca^{2+}, or whether ROS were produced in response to the redox shifts and mitochondrial depolarization. Further experiments will be necessary to determine a consequence of these events.

Mitochondrial cytochrome *c* release plays a key role in the pathway of apoptosis activation [66]. It has been shown that DOX induces remarkable, dose-dependent cytochrome *c* release and execution of the caspase-dependent apoptosis [23]. Cytochrome *c* release from mitochondria can be induced by elevated calcium or ROS and can be blocked by cyclosporin A, pointing to the involvement of permeability transition. Peroxidation of cardiolipin induces cytochrome *c* detachment from the inner mitochondrial membrane and release into the extra-mitochondrial environment. ROS, therefore, may play a key role in mitochondrial cytochrome *c* release [23]. Also, redox state of cytochrome *c* influences its detachment from the inner mitochondrial membrane. Moreover, oxidative damage to respiratory chain may lead to increased ROS production that will induce more cytochrome *c* release. In the same way, loss of cytochrome *c* can stimulate mitochondrial ROS formation, thus providing an amplification effect. Previous reports have shown that cytochrome *c* depletion can lead to a reduction of both mitochondrial membrane potential and respiratory function [67]. However, some studies show that cytochrome *c* release is not directly dependent on mitochondrial membrane depolarization [68] and $\Delta\Psi m$ drop alone seems not enough to induce apoptosis [69]. Also, it is still unclear to which extent apoptotic cytochrome *c* release can diminish mitochondrial respiration. One limitation of this study is that all confocal fluorescent measurements (redox state, $\Delta\Psi m$, calcium) were performed using confluent, attached cells (similar to the normal conditions of cell growing), whereas respirometry and enzymatic analyses always require cells in suspension. This difference may partially explain an apparent discrepancy that brief incubation with DOX significantly decreases mitochondrial membrane potential (up to ~30% of control) without changes in mitochondrial respiration. Another explanation can be related to the important problem of a reversibility of the observed effects after different times of DOX treatment, which certainly deserves further investigation.

Taken together, our data evidence that DOX-induced cell death is associated with mitochondrial respiratory chain defects and reduced levels of cytosolic ATP, but these declines were manifested significantly later after mitochondrial redox state shifts, ROS production, decrease in mitochondrial membrane potential and increased mitochondrial Ca^{2+} levels. New information about distinct effects of doxorubicin on mitochondrial function, as well as their metabolic consequences may provide a rational means of understanding the specific role of mitochondria in chemotherapy and the molecular mechanisms of doxorubicin chemoresistance. Moreover, detecting changes in redox state and other mitochondrial alterations can be useful for detecting chemotherapy responses in vivo. In future the results of this study can be used to develop new methods for evaluating the efficacy of chemotherapy in cancer patients based on an analysis of mitochondria using human biopsies.

Acknowledgement

This work was supported by a research grant from the Austrian Science Fund (FWF): [P 22080-B20].

References

[1] G. Kroemer, J.C. Reed, Mitochondrial control of cell death, Nat. Med. 6 (2000) 513–519.
[2] D.D. Newmeyer, S. Ferguson-Miller, Mitochondria: releasing power for life and unleashing the machineries of death, Cell 112 (2003) 873.
[3] E. Alirol, J.C. Martinou, Mitochondria and cancer: is there a morphological connection? Oncogene 25 (2006) 4706–4716.
[4] J.S. Carew, P. Huang, Mitochondrial defects in cancer, Mol. Cancer 1 (2002) 9.
[5] A. Mayevsky, Mitochondrial function and energy metabolism in cancer cells: past overview and future perspectives, Mitochondrion 9 (2009) 165–179.
[6] M.E. Harper, A. Antoniou, E. Villalobos-Menuey, A. Russo, R. Trauger, M. Vendemelio, A. George, R. Bartholomew, D. Carlo, A. Shaikh, J. Kupperman, E.W. Newell, I.A. Bespalov, S.S. Wallace, Y. Liu, J.R. Rogers, G.L. Gibbs, J.L. Leahy, R.E. Camley, R. Melamede, M.K. Newell, Characterization of a novel metabolic strategy used by drug-resistant tumor cells, FASEB J. 16 (2002) 1550–1557.
[7] F. Arcamone, F. Animati, G. Capranico, P. Lombardi, G. Pratesi, S. Manzini, R. Supino, F. Zunino, New developments in antitumor anthracyclines, Pharmacol. Ther. 76 (1997) 117–124.
[8] G.N. Hortobagyi, Anthracyclines in the treatment of cancer. An overview, Drugs 54 (1997) 1–7.
[9] J.M. Berthiaume, K.B. Wallace, Adriamycin-induced oxidative mitochondrial cardiotoxicity, Cell Biol. Toxicol. 23 (2007) 15–25.
[10] L. Gille, H. Nohl, Analyses of the molecular mechanism of adriamycin-induced cardiotoxicity, Free Radic. Biol. Med. 23 (1997) 775–782.
[11] M.G. Mott, Anthracycline cardiotoxicity and its prevention, Ann. N. Y. Acad. Sci. 824 (1997) 221–228.
[12] S. Rajagopalan, P.M. Politi, B.K. Sinha, C.E. Myers, Adriamycin-induced free radical formation in the perfused rat heart: implications for cardiotoxicity, Cancer Res. 48 (1988) 4766–4769.
[13] K. Shan, A.M. Lincoff, J.B. Young, Anthracycline-induced cardiotoxicity, Ann. Intern. Med. 125 (1996) 47–58.
[14] P.K. Singal, N. Iliskovic, Doxorubicin-induced cardiomyopathy, N. Engl. J. Med. 339 (1998) 900–905.
[15] A.C. Childs, S.L. Phaneuf, A.J. Dirks, T. Phillips, C. Leeuwenburgh, Doxorubicin treatment in vivo causes cytochrome C release and cardiomyocyte apoptosis, as well as increased mitochondrial efficiency, superoxide dismutase activity, and Bcl-2:Bax ratio, Cancer Res. 62 (2002) 4592–4598.
[16] M.E. Clementi, B. Giardina, S.E. Di, A. Mordente, F. Misiti, Doxorubicin-derived metabolites induce release of cytochrome C and inhibition of respiration on cardiac isolated mitochondria, Anticancer Res. 23 (2003) 2445–2450.
[17] K.J. Davies, J.H. Doroshow, Redox cycling of anthracyclines by cardiac mitochondria. I. Anthracycline radical formation by NADH dehydrogenase, J. Biol. Chem. 261 (1986) 3060–3067.
[18] E.J. Demant, Inactivation of cytochrome c oxidase activity in mitochondrial membranes during redox cycling of doxorubicin, Biochem. Pharmacol. 41 (1991) 543–552.
[19] E. Goormaghtigh, R. Brasseur, J.M. Ruysschaert, Adriamycin inactivates cytochrome c oxidase by exclusion of the enzyme from its cardiolipin essential environment, Biochem. Biophys. Res. Commun. 104 (1982) 314–320.
[20] K. Nicolay, K.B. De, Effects of adriamycin on respiratory chain activities in mitochondria from rat liver, rat heart and bovine heart. Evidence for a preferential inhibition of complex III and IV, Biochim. Biophys. Acta 892 (1987) 320–330.
[21] L.C. Papadopoulou, G. Theophilidis, G.N. Thomopoulos, A.S. Tsiftsoglou, Structural and functional impairment of mitochondria in adriamycin-induced cardiomyopathy in mice: suppression of cytochrome c oxidase II gene expression, Biochem. Pharmacol. 57 (1999) 481–489.
[22] J.H. Doroshow, K.J. Davies, Redox cycling of anthracyclines by cardiac mitochondria. II. Formation of superoxide anion, hydrogen peroxide, and hydroxyl radical, J. Biol. Chem. 261 (1986) 3068–3074.
[23] P. Mukhopadhyay, M. Rajesh, S. Batkai, Y. Kashiwaya, G. Hasko, L. Liaudet, C. Szabo, P. Pacher, Role of superoxide, nitric oxide, and peroxynitrite in doxorubicin-induced cell death in vivo and in vitro, Am. J. Physiol. Heart Circ. Physiol. 296 (2009) H1466–H1483.
[24] K. Chandran, D. Aggarwal, R.Q. Migrino, J. Joseph, D. McAllister, E.A. Konorev, W.E. Antholine, J. Zielonka, S. Srinivasan, N.G. Avadhani, B. Kalyanaraman, Doxorubicin inactivates myocardial cytochrome c oxidase in rats: cardioprotection by Mito-Q, Biophys. J. 96 (2009) 1388–1398.
[25] E. Balli, U.O. Mete, A. Tuli, O. Tap, M. Kaya, Effect of melatonin on the cardiotoxicity of doxorubicin, Histol. Histopathol. 19 (2004) 1101–1108.
[26] M. Tokarska-Schlattner, M. Zaugg, S.R. Da, E. Lucchinetti, M.C. Schaub, T. Wallimann, U. Schlattner, Acute toxicity of doxorubicin on isolated perfused heart: response of kinases regulating energy supply, Am. J. Physiol. Heart Circ. Physiol. 289 (2005) H37–H47.
[27] M. Tokarska-Schlattner, M. Zaugg, C. Zuppinger, T. Wallimann, U. Schlattner, New insights into doxorubicin-induced cardiotoxicity: the critical role of cellular energetics, J. Mol. Cell. Cardiol. 41 (2006) 389–405.
[28] C. Friesen, S. Fulda, K.M. Debatin, Induction of CD95 ligand and apoptosis by doxorubicin is modulated by the redox state in chemosensitive- and drug-resistant tumor cells, Cell Death Differ. 6 (1999) 471–480.

[29] Y.J. Jiang, Q. Sun, X.S. Fang, X. Wang, Comparative mitochondrial proteomic analysis of Rji cells exposed to adriamycin, Mol. Med. 15 (2009) 173–182.
[30] A.A. Mhawi, Interaction of doxorubicin with the subcellular structures of the sensitive and Bcl-xL-overexpressing MCF-7 cell line: confocal and low-energy-loss transmission electron microscopy, Micron 40 (2009) 702–712.
[31] A.V. Kuznetsov, D. Strobl, E. Ruttmann, A. Konigsrainer, R. Margreiter, E. Gnaiger, Evaluation of mitochondrial respiratory function in small biopsies of liver, Anal. Biochem. 305 (2002) 186–194.
[32] A.V. Kuznetsov, S. Schneeberger, R. Seiler, G. Brandacher, W. Mark, W. Steurer, V. Saks, Y. Usson, R. Margreiter, E. Gnaiger, Mitochondrial defects and heterogeneous cytochrome c release after cardiac cold ischemia and reperfusion, Am. J. Physiol. Heart Circ. Physiol. 286 (2004) H1633–H1641.
[33] A.V. Kuznetsov, V. Veksler, F.N. Gellerich, V. Saks, R. Margreiter, W.S. Kunz, Analysis of mitochondrial function in situ in permeabilized muscle fibers, tissues and cells, Nat. Protoc. 3 (2008) 965–976.
[34] A.V. Kuznetsov, J. Smigelskaite, C. Doblander, M. Janakiraman, M. Hermann, M. Wurm, S.F. Scheidl, R. Sucher, A. Deutschmann, J. Troppmair, Survival signaling by C-RAF: mitochondrial reactive oxygen species and Ca2+ are critical targets, Mol. Cell. Biol. 28 (2008) 2304–2313.
[35] T. Andrienko, A.V. Kuznetsov, T. Kaambre, Y. Usson, A. Orosco, F. Appaix, T. Tiivel, P. Sikk, M. Vendelin, R. Margreiter, V.A. Saks, Metabolic consequences of functional complexes of mitochondria, myofibrils and sarcoplasmic reticulum in muscle cells, J. Exp. Biol. 206 (2003) 2059–2072.
[36] F. Appaix, A.V. Kuznetsov, Y. Usson, L. Kay, T. Andrienko, J. Olivares, T. Kaambre, P. Sikk, R. Margreiter, V. Saks, Possible role of cytoskeleton in intracellular arrangement and regulation of mitochondria, Exp. Physiol. 88 (2003) 175–190.
[37] S. Huang, A.A. Heikal, W.W. Webb, Two-photon fluorescence spectroscopy and microscopy of NAD(P)H and flavoprotein, Biophys. J. 82 (2002) 2811–2825.
[38] A.V. Kuznetsov, O. Mayboroda, D. Kunz, K. Winkler, W. Schubert, W.S. Kunz, Functional imaging of mitochondria in saponin-permeabilized mice muscle, fibers, J. Cell Biol. 140 (1998) 1091–1099.
[39] H.S. Kim, Y.S. Lee, D.K. Kim, Doxorubicin exerts cytotoxic effects through cell cycle arrest and Fas-mediated cell death, Pharmacology 84 (2009) 300–309.
[40] M.G. Premrov, R. Zenobi, A. Conforti, M.G. Giganti, P. Sinibaldi-Vallebona, Modifications in morphology and size distribution induced by adriamycin in cultured leukemia cells, J. Chemother. 1 (1989) 1154–1156.
[41] N. Sarvazyan, Visualization of doxorubicin-induced oxidative stress in isolated cardiac myocytes, Am. J. Physiol. 271 (1996) H2079–H2085.
[42] H. Mizutani, S. Tada-Oikawa, Y. Hiraku, M. Kojima, S. Kawanishi, Mechanism of apoptosis induced by doxorubicin through the generation of hydrogen peroxide, Life Sci. 76 (2005) 1439–1453.
[43] A. Mayevsky, G.G. Rogatsky, Mitochondrial function in vivo evaluated by NADH fluorescence: from animal models to human studies, Am. J. Physiol. Cell Physiol. 292 (2007) C615–C640.
[44] A. Mayevsky, E. Barbiro-Michaely, Use of NADH fluorescence to determine mitochondrial function in vivo, Int. J. Biochem. Cell Biol. 41 (2009) 1977–1988.
[45] H. Yang, T. Yang, J.A. Baur, E. Perez, T. Matsui, J.J. Carmona, D.W. Lamming, N.C. Souza-Pinto, V.A. Bohr, A. Rosenzweig, C.R. De, A.A. Sauve, D.A. Sinclair, Nutrient-sensitive mitochondrial NAD+ levels dictate cell survival, Cell 130 (2007) 1095–1107.
[46] W.S. Kunz, A.V. Kuznetsov, K. Winkler, F.N. Gellerich, S. Neuhof, H.W. Neumann, Measurement of fluorescence changes of NAD(P)H and of fluorescent flavoproteins in saponin-skinned human skeletal muscle fibers, Anal. Biochem. 216 (1994) 322–327.
[47] W.S. Kunz, K. Winkler, A.V. Kuznetsov, H. Lins, E. Kirches, C.W. Wallesch, Detection of mitochondrial defects by laser fluorimetry, Mol. Cell. Biochem. 174 (1997) 97–100.
[48] A.V. Kuznetsov, S. Schneeberger, O. Renz, H. Meusburger, V. Saks, Y. Usson, R. Margreiter, Functional heterogeneity of mitochondria after cardiac cold ischemia and reperfusion revealed by confocal imaging, Transplantation 77 (2004) 754–756.
[49] A. Serafino, P. Sinibaldi-Vallebona, G. Lazzarino, B. Tavazzi, P.D. Di, G. Rasi, G. Ravagnan, Modifications of mitochondria in human tumor cells during anthracycline-induced apoptosis, Anticancer Res. 20 (2000) 3383–3394.
[50] O.F. De, C. Chauvin, X. Ronot, M. Mousseau, X. Leverve, E. Fontaine, Effects of permeability transition inhibition and decrease in cytochrome c content on doxorubicin toxicity in K562 cells, Oncogene 25 (2006) 2646–2655.
[51] L. Galluzzi, N. Larochette, N. Zamzami, G. Kroemer, Mitochondria as therapeutic targets for cancer chemotherapy, Oncogene 25 (2006) 4812–4830.
[52] E. Chacon, D. Acosta, Mitochondrial regulation of superoxide by Ca2+: an alternate mechanism for the cardiotoxicity of doxorubicin, Toxicol. Appl. Pharmacol. 107 (1991) 117–128.
[53] E. Chacon, R. Ulrich, D. Acosta, A digitized-fluorescence-imaging study of mitochondrial Ca2+ increase by doxorubicin in cardiac myocytes, Biochem. J. 281 (1992) 871–878.
[54] L.E. Solem, T.R. Henry, K.B. Wallace, Disruption of mitochondrial calcium homeostasis following chronic doxorubicin administration, Toxicol. Appl. Pharmacol. 129 (1994) 214–222.
[55] P.S. Green, C. Leeuwenburgh, Mitochondrial dysfunction is an early indicator of doxorubicin-induced apoptosis, Biochim. Biophys. Acta 1588 (2002) 94–101.
[56] D. Cheneval, M. Muller, E. Carafoli, The mitochondrial phosphate carrier reconstituted in liposomes is inhibited by doxorubicin, FEBS Lett. 159 (1983) 123–126.
[57] M. Muller, D. Cheneval, E. Carafoli, Doxorubicin inhibits the phosphate-transport protein reconstituted in liposomes. A study on the mechanism of the inhibition, Eur. J. Biochem. 140 (1984) 447–452.
[58] P.J. Oliveira, K.B. Wallace, Depletion of adenine nucleotide translocator protein in heart mitochondria from doxorubicin-treated rats—relevance for mitochondrial dysfunction, Toxicology 220 (2006) 160–168.
[59] E. Goormaghtigh, P. Huart, M. Praet, R. Brasseur, J.M. Ruysschaert, Structure of the adriamycin–cardiolipin complex. Role in mitochondrial toxicity, Biophys. Chem. 35 (1990) 247–257.
[60] Z. Tao, H.G. Withers, H.S. Penefsky, J. Goodisman, A.K. Souid, Inhibition of cellular respiration by doxorubicin, Chem. Res. Toxicol. 19 (2006) 1051–1058.
[61] A.K. Souid, H.S. Penefsky, P.D. Sadowitz, B. Toms, Enhanced cellular respiration in cells exposed to doxorubicin, Mol. Pharm. 3 (2006) 307–321.
[62] A.K. Souid, K.A. Tacka, K.A. Galvan, H.S. Penefsky, Immediate effects of anticancer drugs on mitochondrial oxygen consumption, Biochem. Pharmacol. 66 (2003) 977–987.
[63] E. Goormaghtigh, G. Pollakis, J.M. Ruysschaert, Mitochondrial membrane modifications induced by adriamycin-mediated electron transport, Biochem. Pharmacol. 32 (1983) 889–893.
[64] R. Asmis, Y. Wang, L. Xu, M. Kisgati, J.G. Begley, J.J. Mieyal, A novel thiol oxidation-based mechanism for adriamycin-induced cell injury in human macrophages, FASEB J. 19 (2005) 1866–1868.
[65] B.K. Sinha, E.G. Mimnaugh, S. Rajagopalan, C.E. Myers, Adriamycin activation and oxygen free radical formation in human breast tumor cells: protective role of glutathione peroxidase in adriamycin resistance, Cancer Res. 49 (1989) 3844–3848.
[66] R.M. Kluck, E. Bossy-Wetzel, D.R. Green, D.D. Newmeyer, The release of cytochrome c from mitochondria: a primary site for Bcl-2 regulation of apoptosis, Science 275 (1997) 1132–1136.
[67] A. Krippner, A. Matsuno-Yagi, R.A. Gottlieb, B.M. Babior, Loss of function of cytochrome c in Jurkat cells undergoing fas-mediated apoptosis, J. Biol. Chem. 271 (1996) 21629–21636.
[68] E. Bossy-Wetzel, D.D. Newmeyer, D.R. Green, Mitochondrial cytochrome c release in apoptosis occurs upstream of DEVD-specific caspase activation and independently of mitochondrial transmembrane depolarization, EMBO J. 17 (1998) 37–49.
[69] R. Dey, C.T. Moraes, Lack of oxidative phosphorylation and low mitochondrial membrane potential decrease susceptibility to apoptosis and do not modulate the protective effect of Bcl-x(L) in osteosarcoma cells, J. Biol. Chem. 275 (2000) 7087–7094.